

# Controlling crystal symmetries in phase-field crystal models

Kuo-An Wu<sup>1</sup>, Mathis Plapp<sup>2</sup> and Peter W Voorhees<sup>1,3</sup>

<sup>1</sup> Department of Materials Science and Engineering, Northwestern University, Evanston, Illinois 60208, USA

<sup>2</sup> Physique de la Matière Condensée, École Polytechnique, CNRS, 91128 Palaiseau, France

<sup>3</sup> Department of Engineering Sciences and Applied Mathematics, Northwestern University, Evanston, Illinois 60208, USA

E-mail: mathis.plapp@polytechnique.fr, kuoan-wu@northwestern.edu, p-voorhees@northwestern.edu

## Abstract.

We investigate the possibility to control the symmetry of ordered states in phase-field crystal models by tuning nonlinear resonances. In two dimensions, we find that a state of square symmetry as well as coexistence between squares and hexagons can be easily obtained. In contrast, it is delicate to obtain coexistence of squares and liquid. We develop a general method for constructing free energy functionals that exhibit solid-liquid coexistence with desired crystal symmetries. As an example, we develop a free energy functional for square-liquid coexistence in two dimensions. A systematic analysis for determining the parameters of the necessary nonlinear terms is provided. The implications of our findings for simulations of materials with simple cubic symmetry are discussed.

PACS numbers: 68.08.-p, 45.70.Qj, 47.54.-r, 81.16.Rf

## 1. Introduction

The phase-field crystal (PFC) model has rapidly gained popularity in recent years as a potentially powerful tool to simulate the evolution of materials with atomistic resolution on time scales that are orders of magnitude larger than those that can be attained by molecular dynamics simulations. While it was originally [1, 2] inspired by phenomenological equations developed in the general context of pattern formation [3, 4], it has now been established [5, 6, 7] that it can be obtained as a simplification of classical density functional theory (DFT) of freezing [8, 9].

To make the PFC model useful for practical applications in materials science, it has to be established how the model parameters need to be chosen in order to reproduce the physical properties of a given material as closely as possible. This is currently a very active area of research, and several contributions of the present volume are dedicated

to this subject. One of the most fundamental properties of a material is of course its crystal structure. As detailed below, the original PFC model [1, 2] contains only two parameters: a scaled global density  $\bar{\psi}$  and a scaled temperature  $\epsilon$ . The latter indicates the distance to the critical point of the PFC model, which is located at  $\bar{\psi} = \epsilon = 0$ . For small  $\epsilon$ , the PFC model exhibits, besides the unstructured liquid phase, periodic solutions of nematic (stripe) and hexagonal symmetry in two dimensions, and of bcc symmetry in three dimensions. Recently, it was found that for larger values of  $\epsilon$ , fcc and hcp structure also exist in three dimensions [10, 11, 12]. However, the parameter  $\epsilon$  also controls several other properties of the model, such as the width of the solid-liquid interfaces and their interfacial free energy. Since, to match a given material, these quantities need to be adjusted independently, more degrees of freedom are needed in the model.

It turns out that it is not straightforward to obtain periodic ground states with symmetries that differ from the “natural” ones. This is due to the physics which governs the formation of periodic states in the PFC model: the liquid state is unstable with respect to the formation of periodic solutions if their wavelength falls within a narrow band centred around a characteristic length scale. The periodic density patterns that correspond to crystalline phases are stabilised by nonlinear terms, which lead to the interaction (resonance) of density waves with different unstable wave vectors. The hexagon/bcc and stripe patterns arise from the simplest nonlinearities involving triadic and quartic resonances of wave vectors with equal modulus, respectively, which explains their ubiquity in nature [4]. This also naturally explains why new structures appear for larger values of  $\epsilon$  [10, 11, 12]: since the range of unstable wavelengths increases with  $\epsilon$ , new resonances become possible.

A way to control the selection of crystal structures is thus to modify the nonlinear resonances. Two ways to do this have been explored in the literature, both inspired by earlier work in the physics of pattern formation. The first idea is to make *two* bands of wavelengths unstable, and to use the ratio between the two characteristic wavelengths as an additional geometric parameter which allows to stabilise patterns of a certain symmetry [13]. Using this approach, PFC models with a ground state of fcc symmetry were recently developed [14, 15]. While these models are robust and versatile, they have two potential drawbacks, namely (i) in the analogy with DFT, the two distinct length scales should arise from two distinct peaks in the liquid structure factor; for the simplest version of the model, a structure factor that is very different from those typically measured has to be used, and (ii) the equation of motion for the density field contains spatial derivatives of up to 10th order, which makes simulations in geometries that cannot easily be handled in reciprocal space very cumbersome.

The second approach, which will be our main focus, is to add new nonlinear terms to the model which modify the strength of the resonances and can thus favour patterns of different symmetries. Here, we will restrict our investigations to two dimensions, where the obvious missing state is a square pattern. The question of how a square pattern can arise from a rotationally invariant homogeneous state has been extensively studied in

the context of convection patterns [16], because squares can be observed under certain experimental conditions. It has been demonstrated that simple additional nonlinearities can stabilise squares [17, 18], and that squares can coexist with hexagons [19, 20]. These phenomenological equations have already been used to study the transition from hexagonal to square symmetry upon a change of the control parameters, in a spirit very close to the one of the PFC model, before that name was actually coined [21, 22]. The geometric properties of grain boundaries between two domains of square symmetries have also been studied [23]. Finally, isolated patches of squares in coexistence with the unstructured state (“oscillons”) have also been found in similar equations [24, 25].

Here, we investigate whether it is possible to use this approach to design a simple and robust PFC model with square symmetry. We find that it is indeed straightforward to obtain squares as well as coexistence of squares and hexagons following the recipes found in the literature. In contrast, square-liquid coexistence can only be obtained with a combination of several nonlinear terms and carefully tuned parameters. We develop a systematic approach to determine suitable parameter ranges that yield stable square-liquid interfaces, and confirm our analytic calculations by numerical simulations. We also evaluate the elastic coefficients of the square solid for the parameters used in the simulations.

The remainder of the paper is organised as follows. In Section 2, we define the model and recall the calculation of nonlinear resonances and the resulting selection of symmetry. In Section 3 we calculate the free energies of the various periodic patterns in a generalised PFC model in two dimensions, with particular emphasis on square-liquid coexistence. Section 4 presents the comparison between our analytic results and numerical calculations; the elastic coefficients are evaluated in Section 5, and Section 6 gives a brief conclusion.

## 2. The model

### 2.1. General considerations

For the purpose of exposition, we start with the standard PFC model [1, 2], which has the dimensionless free energy functional

$$F = \int d\vec{r} \left\{ \frac{\psi}{2} [-\epsilon + (\nabla^2 + 1)^2] \psi + \frac{\psi^4}{4} \right\}, \quad (1)$$

where  $\psi$  is a dimensionless particle density measured from a constant reference value, and  $\epsilon$  is a constant. This form of the free energy functional was originally proposed by Swift and Hohenberg as a phenomenological description of patterns that emerge in various hydrodynamical systems [3]. In this context,  $\epsilon$  is the distance from the bifurcation threshold at which the unstructured (quiescent) state becomes unstable. We have used dimensionless units in which the modulus of the characteristic wave number is unity, and energy and time have been scaled by appropriate quantities as detailed in [6]. The manner by which this free energy functional and its parameters can be related to classical

DFT is detailed in [5, 6, 7] and need not be repeated here.

In the original Swift-Hohenberg equation,  $\psi$  is a linear combination of the deviations of the temperature and velocity fields from the quiescent state. It is treated as a non-conserved order parameter, and thus the system is free to evolve towards the global free energy minimum. In contrast, in the PFC model the field  $\psi$  is a local particle density and hence a conserved quantity. This provides an additional control parameter, namely, the average density  $\bar{\psi} \equiv \int \psi d\vec{r} / \int d\vec{r}$ .

The free energy of periodic states can be evaluated using the one-mode approximation, in which the density field is given by a sum of density waves,

$$\psi(\vec{r}) = \bar{\psi} + \delta\psi(\vec{r}) = \bar{\psi} + \sum_j A_{\vec{K}_j} \exp(i\vec{K}_j \cdot \vec{r}) = \bar{\psi} + A \sum_j \exp(i\vec{K}_j \cdot \vec{r}), \quad (2)$$

where  $\vec{K}_j$  are the principal reciprocal lattice vectors of the considered structure (with  $|\vec{K}_j| \equiv q$ ), and  $A$  is the amplitude of the density waves, where we have used the fact that for a homogeneous solid all density waves have the same amplitude,  $|A_{\vec{K}_j}| = A$ . This ansatz is inserted into the free energy functional, and the result is integrated over one unit cell. In this procedure, all terms that contain oscillatory exponential factors integrate out, and only the products of exponentials in which two, three, or four of the  $\vec{K}_j$ 's sum up to zero contribute to the final result. Thus, non-trivial contributions arise from the triadic and quartic resonances. Whereas the latter can generate stripes (or squares, see below), hexagonal and bcc ordered phases are stabilised by triadic resonances because the principal reciprocal lattice vectors are able to form ‘‘triads’’ (i.e., closed triangles, for example,  $\langle 110 \rangle$ ,  $\langle \bar{1}01 \rangle$  and  $\langle 0\bar{1}\bar{1} \rangle$  for bcc lattices). The cubic terms that are needed for triadic resonances to occur are generated by the expansion of the  $\psi^4$  term:  $(\bar{\psi} + \delta\psi)^4 = (\delta\psi)^4 + 4\bar{\psi}(\delta\psi)^3 + \dots$ . Therefore, they are absent for  $\bar{\psi} = 0$  and become increasingly important with increasing  $|\bar{\psi}|$ . This explains the sequence of phases found in the phase diagram of the PFC model [2] with increasing  $|\bar{\psi}|$ : rolls (stripes)  $\rightarrow$  hexagons  $\rightarrow$  liquid in two dimensions, and rolls  $\rightarrow$  hexagons  $\rightarrow$  bcc  $\rightarrow$  liquid in three dimensions. In addition, since the free energy expressed in terms of  $A$  contains terms in  $A^2$ ,  $A^3$ , and  $A^4$ , the bifurcation from liquid to hexagons can be transcritical, and a first-order transition from liquid to hexagons/bcc with a finite coexistence zone in  $\bar{\psi}$  is possible. In contrast, for crystals with square, simple-cubic and face-centred-cubic lattices, no triads can be formed, and the free energy contains only terms in  $A^2$  and  $A^4$ . This makes the transition from liquid to squares supercritical, and it was shown by weakly nonlinear analysis [6, 14] that solid-liquid coexistence is impossible under these conditions.

From the above considerations, we can conclude that the model has to fulfil three requirements in order to obtain square-liquid coexistence. First, the quartic resonances need to favour squares rather than stripes, second the transition from squares to liquid must be subcritical to give rise to solid-liquid coexistence, and third the square state must have a lower free energy than hexagons even in the presence of triadic resonances that occur for  $\bar{\psi} \neq 0$ . We will address these questions in the following, and we will develop a systematic approach to determine coefficients that favour periodic states with

cubic symmetry.

## 2.2. Anisotropic terms

Let us first discuss nonlinear terms that can be used to favour squares in two dimensions. To this end, it is useful to consider rhombi, that is, a density field composed just of two sets of density waves with wave vectors  $\pm\vec{K}_1$  and  $\pm\vec{K}_2$ , which have equal magnitude  $q$  and form an arbitrary angle  $\theta$  between them,

$$\delta\psi(\vec{r}) = A [\exp(i\vec{K}_1 \cdot \vec{r}) + \exp(i\vec{K}_2 \cdot \vec{r}) + c.c.]. \quad (3)$$

Obviously, there are no triadic resonances. The quartic resonances generated by the  $\psi^4$  term in equation (1) give a result that is independent of  $\theta$ . Thus, this term does not favour any particular symmetry.

One possibility of an ‘‘anisotropic’’ term, used in the literature [18, 19, 20], is a term proportional to  $\psi^2\Delta^2\psi^2$ , where  $\Delta = \nabla^2$  is the Laplace operator. Here, we consider a more general set of nonlinear terms of the form  $g_{2n}\psi^2\Delta^n\psi^2$  in the free energy functional, where  $g_{2n}$  are constant coefficients. Following the procedure outlined above, we obtain

$$g_{2n} \int d\vec{r} \psi^2 \Delta^n \psi^2 = g_{2n} \int d\vec{r} \left( \bar{\psi}^2 \Delta^n (\delta\psi)^2 + 4\bar{\psi}^2 \delta\psi \Delta^n \delta\psi + 2\bar{\psi} \delta\psi \Delta^n (\delta\psi)^2 + 2\bar{\psi} (\delta\psi)^2 \Delta^n \delta\psi + (\delta\psi)^2 \Delta^n (\delta\psi)^2 \right). \quad (4)$$

Substituting equation (3) into equation (4) yields

$$\frac{g_{2n}}{V} \int d\vec{r} \psi^2 \Delta^n \psi^2 = (-1)^n g_{2n} \left[ 8\bar{\psi}^2 A^2 (|\vec{K}_1|^{2n} + |\vec{K}_2|^{2n}) + 2A^4 (|2\vec{K}_1|^{2n} + |2\vec{K}_2|^{2n} + 4|\vec{K}_1 + \vec{K}_2|^{2n} + 4|\vec{K}_1 - \vec{K}_2|^{2n}) \right], \quad (5)$$

where  $V = \int d\vec{r}$  is the volume of one unit cell. Together with the vector addition properties illustrated in Figure 1,

$$\begin{aligned} |\vec{K}_1 + \vec{K}_2| &= 2q \cos \frac{\theta}{2} \\ |\vec{K}_1 - \vec{K}_2| &= 2q \sin \frac{\theta}{2}, \end{aligned} \quad (6)$$

equation (5) can be rewritten as

$$\begin{aligned} \frac{g_{2n}}{V} \int d\vec{r} \psi^2 \Delta^n \psi^2 &= (-1)^n g_{2n} q^{2n} \left[ (16\bar{\psi}^2 A^2 + 2^{2n+2} A^4) + 8A^4 \left( \cos^{2n} \frac{\theta}{2} + \sin^{2n} \frac{\theta}{2} \right) \right] \\ &= f_{\text{isotropic}} + f_{\text{anisotropic}}. \end{aligned} \quad (7)$$

where

$$f_{\text{isotropic}} \equiv (-1)^n g_{2n} q^{2n} (16\bar{\psi}^2 A^2 + 2^{2n+2} A^4) \quad (8)$$

is independent of the angle  $\theta$ , but depends on  $\bar{\psi}$ , and the anisotropic part of the free energy that depends on the angle and thus on the symmetry of the pattern is

$$f_{\text{anisotropic}} \equiv 8(-1)^n g_{2n} q^{2n} A^4 \left( \cos^{2n} \frac{\theta}{2} + \sin^{2n} \frac{\theta}{2} \right). \quad (9)$$

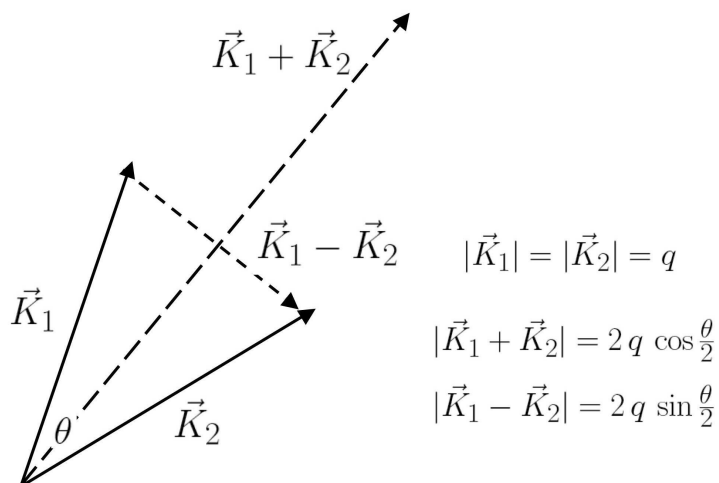


**Figure 1.** Terms of the form  $\psi^2 \Delta^n \psi^2$  give rise to a  $\theta$ -dependent free energy through the above vector addition operations.

For  $n = 1$ , the dependence on  $\theta$  in the anisotropic part vanishes because of the trigonometric identity  $\cos^2(\theta/2) + \sin^2(\theta/2) = 1$ . However, for  $n = 2$ , the anisotropic part of the free energy is a simple function of  $\theta$  which is minimised by  $\theta = \pi/2$  if  $g_4 > 0$  and by  $\theta = 0$  if  $g_4 < 0$ . Similar results are obtained for  $n = 3$ ; however, the square symmetry is favoured when  $g_6 < 0$ . It is interesting to note that for  $n \geq 4$ , the anisotropic part of the free energy contains higher order harmonics, which suggests a possible means to favour arbitrary angles between density waves by an appropriate combination of such terms.

Another type of nonlinearity used in the literature [17, 21, 22] to favour squares is  $|\nabla\psi|^4$ . Indeed, repeating the above calculation for rhombi with a term of the form  $s_4|\nabla\psi|^4/4$  with  $s_4$  a constant, we find

$$\frac{s_4}{V} \int d\vec{r} \frac{1}{4} |\nabla\psi|^4 = s_4 q^4 A^4 (5 + \cos^2 \theta) \quad (10)$$

which can again be split in an isotropic and an anisotropic part. The anisotropic part is minimised for  $\theta = \pi/2$  if  $s_4 > 0$ . Note that, in this case, the isotropic part does not depend on  $\bar{\psi}$ .

The above calculations are valid both in two and three dimensions. In three dimensions, an angle of  $\pi/2$  between density waves corresponds to a simple cubic structure, which can therefore be obtained in a straightforward manner using this method.

### 2.3. Subcritical bifurcation

For crystal structures without triadic interactions, since to lowest order the free energy can be expressed in even powers of  $A$ , a subcritical bifurcation is required for solid-liquid

coexistence. The generic form of a free energy that exhibits a subcritical bifurcation is

$$f = \alpha A^2 - \beta A^4 + \gamma A^6 \quad (11)$$

where  $\beta$  and  $\gamma$  are positive. The parameter  $\alpha$  controls the growth rate of small perturbations of the liquid state (linear stability); the liquid is stable for  $\alpha > 0$ . The  $\psi^4$  term in the standard PFC free energy functional shown in equation (1) results in a  $\bar{\psi}$ -dependent quadratic coefficient. Within the one-mode approximation, for this model  $\alpha \sim -\epsilon + (1 - q^2)^2 + 3\bar{\psi}^2$  for density waves with wave number  $q$ .

All nonlinear terms discussed so far yield contributions up to order  $A^4$ . To obtain the necessary contribution in  $A^6$ , some higher order nonlinearity needs to be added. An obvious possibility would be just  $\psi^6$ , which was indeed used in [24, 25] to model oscillons. The problem with this choice is that for  $\bar{\psi} \neq 0$  it generates additional cubic and quintic terms in the free energy that tend to lower the free energy for hexagonal and bcc phases. As a consequence, this nonlinearity tends to generate the sequence squares  $\rightarrow$  hexagons  $\rightarrow$  liquid in the phase diagram; this was the case for all the cases that we have investigated.

An alternative choice, which will be made in the following, is to add  $s_6|\nabla\psi|^6/6$  to the free energy, which generates terms of order  $A^6$ , but no additional terms depending on  $\bar{\psi}$ . As will be shown below, it is indeed possible to generate a subcritical bifurcation that favours squares by using both  $s_4|\nabla\psi|^4/4$  and  $s_6|\nabla\psi|^6/6$  with  $s_4 < 0$  and  $s_6 > 0$ . However, the resulting square-liquid equilibrium is metastable, whereas the state of lowest energy are hexagons. In order to be able to adjust the respective energies of these states, we must also include the nonlinear terms of the form  $\psi^2\Delta^2\psi^2$  and  $\psi^2\Delta^3\psi^2$  discussed previously. The procedure how to choose appropriate coefficients for all these terms will be detailed in the next section.

### 3. Selection of crystal symmetry

#### 3.1. Free energies

The free energy functional considered in the following is

$$F = \int d\vec{r} \left( \frac{\psi}{2} \left[ -\epsilon + (\nabla^2 + 1)^2 \right] \psi + \frac{\psi^4}{4} + \frac{g_4}{4} \psi^2 \Delta^2 \psi^2 + \frac{g_6}{4} \psi^2 \Delta^3 \psi^2 + \frac{s_4}{4} |\nabla\psi|^4 + \frac{s_6}{6} |\nabla\psi|^6 \right). \quad (12)$$

In two dimensions, the competing patterns are rolls, squares and hexagons. The corresponding density fields in the one-mode approximation of equation (2) are

$$\begin{aligned} \psi_{\text{roll}}(\vec{r}) &= \bar{\psi} + 2A \cos(qx), \\ \psi_{\text{square}}(\vec{r}) &= \bar{\psi} + 2A (\cos qx + \cos qy), \\ \psi_{\text{hex}}(\vec{r}) &= \bar{\psi} + 2A \left( 2 \cos \frac{qx}{2} \cos \frac{\sqrt{3}qy}{2} + \cos qx \right), \end{aligned} \quad (13)$$

where we recall that  $q$  is the magnitude of the principal reciprocal lattice vectors. The free energy is computed by substituting equation (13) into equation (12) and integrating

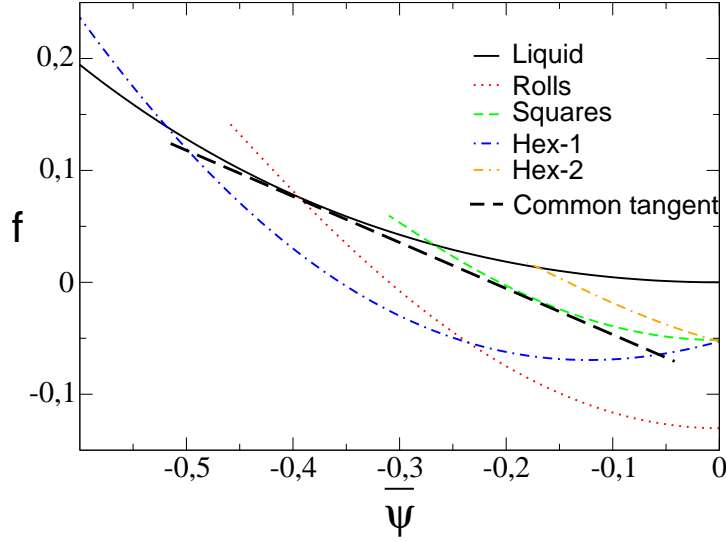


**Figure 2.** Free energy as a function of  $\bar{\psi}$  for  $(s_4, s_6) = (-2, 1)$ ,  $(g_4, g_6) = (0, 0)$  and  $\epsilon = 0.1$ . A common tangent line between the liquid and square free energy curves is drawn (thick dashed line) to illustrate the existence of a wide coexistence region.

over one unit cell, which yields

$$f_{\text{roll}} = f_L + \left( -\epsilon + (1 - q^2)^2 + (3 + 2g_4q^4 - 2g_6q^6)\bar{\psi}^2 \right) A^2 - \frac{1}{2} \left( -3 - 3s_4q^4 - 16g_4q^4 + 64g_6q^6 \right) A^4 + \frac{10}{3} s_6q^6 A^6, \quad (14)$$

$$f_{\text{square}} = f_L + 2 \left( -\epsilon + (1 - q^2)^2 + (3 + 2g_4q^4 - 2g_6q^6)\bar{\psi}^2 \right) A^2 - \left( -9 - 5s_4q^4 - 32g_4q^4 + 96g_6q^6 \right) A^4 + \frac{56}{3} s_6q^6 A^6, \quad (15)$$

$$f_{\text{hex}} = f_L + 3 \left( -\epsilon + (1 - q^2)^2 + (3 + 2g_4q^4 - 2g_6q^6)\bar{\psi}^2 \right) A^2 + 12\bar{\psi} \left( 1 + g_4q^4 - g_6q^6 \right) A^3 - \left( -\frac{45}{2} - \frac{27}{2} s_4q^4 - 84g_4q^4 + 264g_6q^6 \right) A^4 + 91s_6q^6 A^6, \quad (16)$$

where  $f$  is the free energy density,  $f \equiv F/V$ , and  $f_L = (-\epsilon + 1)\bar{\psi}^2/2 + \bar{\psi}^4/4$  is the free energy density of the liquid. The values of  $A$  and  $q$  are determined by minimising the above free energy with respect to  $A$  and  $q$ . One important difference with respect to the standard PFC model should be noted. In the latter,  $q$  appears only in the gradient term. Therefore,  $q$  and  $A$  decouple, and the value of  $q$  that minimises the free energy is always equal to unity. In contrast, the new terms introduce nonlinear couplings between  $A$  and  $q$ , which implies that both quantities depend in a nontrivial way on the parameters. The values of  $q$  and  $A$  which minimise  $f$  are found numerically for each structure using the Newton-Raphson method and are then substituted into equations (14), (15) and (16) to obtain the free energy density for different patterns.



Let us first check whether square-liquid coexistence can be obtained using only the terms proportional to  $s_4$  and  $s_6$ . In figure 2 we plot the free energies of squares and liquid for  $(s_4, s_6) = (-2, 1)$ ,  $(g_4, g_6) = (0, 0)$ , and  $\epsilon = 0.1$ . The common-tangent construction shows that there indeed exists a wide coexistence region as a result of the bifurcation being subcritical. However, the square-liquid coexistence is metastable for these parameters, since both the roll and the hexagonal phases have a lower energy, as shown in figure 2. Note that, since the cubic term which generates hexagons breaks the symmetry between  $A$  and  $-A$ , there are two distinct hexagon solutions that correspond to different values of  $A$ , which are labelled as “Hex-1” and “Hex-2” respectively in the graphs. To modify this ordering of the free energies, we need to include the terms proportional to  $g_4$  and  $g_6$ . In the following, we give a systematic procedure to choose appropriate values for the coefficients.

### 3.2. Rolls vs. squares

We first consider the stability of rolls and squares. As discussed previously, choosing the coefficients of the anisotropic terms of the right sign favours squares. However, for fixed coefficients, the relative energies of the phases may still depend on the value of  $\bar{\psi}$ . Since the solid-liquid coexistence occurs near the density at which the solid and liquid free energy curves intersect, stable square-liquid coexistence is only possible if the intersection of the square and liquid free energy curves occurs at a larger value of  $|\bar{\psi}|$  than the one for rolls and liquid. The following analysis focuses on determining the conditions for the nonlinear coefficients for which this is the case.

The principal reciprocal lattice vectors of rolls and squares cannot form triads; thus, the free energy density of rolls and squares has the general form for a subcritical bifurcation given by equation (11),

$$f_S = f_L + \alpha A^2 - \beta A^4 + \gamma A^6, \quad (17)$$

where the subscript  $S$  (solid) denotes rolls or squares. The solid and liquid free energy curves intersect when the free energy difference of solid and liquid becomes zero,  $\delta f \equiv f_S - f_L = \alpha A^2 - \beta A^4 + \gamma A^6 = 0$ . In addition, the free energy of the solid must be minimised with respect to  $A$ , which yields  $(\partial \delta f / \partial A) = 2\alpha A - 4\beta A^3 + 6\gamma A^5 = 0$ . These two relations yield

$$\alpha = \frac{\beta^2}{4\gamma}. \quad (18)$$

Comparing equations (14), (15) and (16) to equation (17), we obtain

$$\alpha = N \left( -\epsilon + (1 - q^2)^2 + \Gamma \bar{\psi}^2 \right), \quad (19)$$

where

$$\Gamma \equiv 3 + 2g_4 q^4 - 2g_6 q^6, \quad (20)$$

and  $N = 1, 2$  and  $3$  for rolls, squares and hexagons, respectively. Since the exponential growth rate of perturbations with wave number  $q$  is proportional to  $-\alpha$ , in order to

obtain an unconditionally stable liquid at large values of  $|\bar{\psi}|$ ,  $\alpha$  must have a finite lower bound which leads to

$$\Gamma > 0. \quad (21)$$

The intersection of solid and liquid free energy curves is obtained by combining equations (18) and (19), which yields

$$\bar{\psi}^{\text{int}} = -\frac{1}{\sqrt{\Gamma}} \left( \epsilon - (1 - q^2)^2 + \frac{\beta^2}{4N\gamma} \right)^{1/2}. \quad (22)$$

The wave numbers  $q$  that minimise the free energy of rolls and squares are different. However, for large values of  $s_6$  this difference is small so that we can safely neglect it. Under this assumption, the intersection point of solid and liquid free energy curves is solely dictated by the value of  $\beta^2/(4N\gamma)$ . The condition that  $|\bar{\psi}_{\text{square}}^{\text{int}}| > |\bar{\psi}_{\text{roll}}^{\text{int}}|$  then yields inequalities between the coefficients which are given in the appendix. The most important result is that this condition can only be satisfied if  $g_6$  is non-zero.

### 3.3. Hexagons

For hexagons, the free energy contains a cubic term due to triadic interactions,

$$f_{\text{hex}} = f_L + \alpha A^2 + \tau A^3 - \beta A^4 + \gamma A^6, \quad (23)$$

where

$$\begin{aligned} \alpha &= 3 \left( -\epsilon + (1 - q^2)^2 + \Gamma \bar{\psi}^2 \right) \\ \tau &= 6\bar{\psi}(\Gamma - 1) \\ \beta &= -\frac{45}{2} - \frac{27}{2}s_4q^4 - 84g_4q^4 + 264g_6q^6 \\ \gamma &= 91s_6q^6 \end{aligned} \quad (24)$$

In the standard PFC model, the cubic term changes the bifurcation from supercritical to transcritical which not only make hexagons the favoured phase, but also makes hexagon-liquid coexistence possible in the limit of a weakly first-order freezing transition. The cubic term plays a similar role in the subcritical case: it lowers the free energy for hexagons by an amount proportional to  $|\bar{\psi}|$ . In order to make square symmetries favourable, we require the cubic coefficient  $\tau$  to be small for  $\bar{\psi}$  close to the square-liquid coexistence region. Then, the subcritical bifurcation analysis developed in the previous section still gives a good estimate of the intersection points for the free energy curves of hexagons and liquid and can thus be used to evaluate the relative stability of squares and hexagons.

This requirement on  $\tau$  and the condition for a stable liquid are illustrated graphically in figure 3 for  $(g_4, g_6) = (-3.0, -2.1)$ . The condition that the liquid remains linearly stable for large values of  $\bar{\psi}$  requires that  $\Gamma > 0$ . The cubic coefficient  $\tau$  is a function of  $q$  and proportional to the distance between the solid and dashed lines in figure 3. We set  $(s_4, s_6) = (-25, 600)$  and  $\epsilon = 0.001$  so that these parameters satisfy the conditions for a subcritical bifurcation and for  $|\bar{\psi}_{\text{square}}^{\text{int}}| > |\bar{\psi}_{\text{roll}}^{\text{int}}|$  as shown in

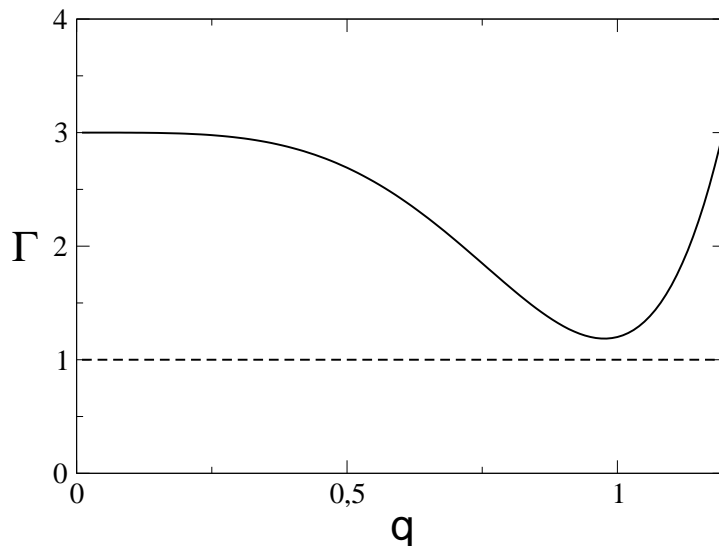


**Figure 3.**  $\Gamma = 3 + 2g_4q^4 - 2g_6q^6$  (solid line) for  $(g_4, g_6) = (-3, -2.1)$ . The condition for a stable liquid is satisfied since  $\Gamma$  is positive. The cubic coefficient  $\tau = 6\bar{\psi}(\Gamma - 1)$  is proportional to the distance between the solid and dashed lines.

equations (A.5) and (A.7) in the appendix. The wave number  $q$  is about 0.98 near the coexistence region, for which the cubic coefficient  $\tau$  is small as shown in figure 3. We can then estimate  $|\bar{\psi}_{\text{hex}}^{\text{int}}|$  using the above analysis for a subcritical bifurcation by assuming  $\tau \approx 0$ ; details can be found in the appendix. For the parameters chosen above, both  $|\bar{\psi}_{\text{roll}}^{\text{int}}|$  and  $|\bar{\psi}_{\text{hex}}^{\text{int}}|$  have smaller values than  $|\bar{\psi}_{\text{square}}^{\text{int}}|$ . These parameters are used in the following numerical simulations.

#### 4. Comparison of analytical solutions and numerical simulations

For a conserved order parameter  $\psi$ , the evolution equation for the free energy functional shown in equation (12) is

$$\begin{aligned} \frac{\partial \psi}{\partial t} &= \nabla^2 \frac{\delta F}{\delta \psi} \\ &= \nabla^2 \left( [-\epsilon + (\nabla^2 + 1)^2] \psi + \psi^3 + g_4 \psi \Delta^2 \psi^2 + g_6 \psi \Delta^3 \psi^2 \right. \\ &\quad \left. - s_4 \nabla \cdot (|\nabla \psi|^2 \nabla \psi) - s_6 \nabla \cdot (|\nabla \psi|^4 \nabla \psi) \right). \end{aligned} \quad (25)$$

Since the main focus of this paper is the stability of crystal symmetries at equilibrium, we use a nonlocal globally conserved dynamics [26] to accelerate the search of equilibrium solutions,

$$\frac{\partial \psi}{\partial t} = -\frac{\delta F}{\delta \psi} + \frac{1}{V} \int d\vec{r} \frac{\delta F}{\delta \psi}. \quad (26)$$

We set the simulation parameters in two dimensions to be  $(g_4, g_6) = (-3.0, -2.1)$ ,  $(s_4, s_6) = (-25, 600)$ ,  $\epsilon = 0.001$ , and the grid spacings  $\Delta x$  and  $\Delta y$  close to 0.5. Numerical simulations are carried out using equation (26) for rolls, squares and hexagons

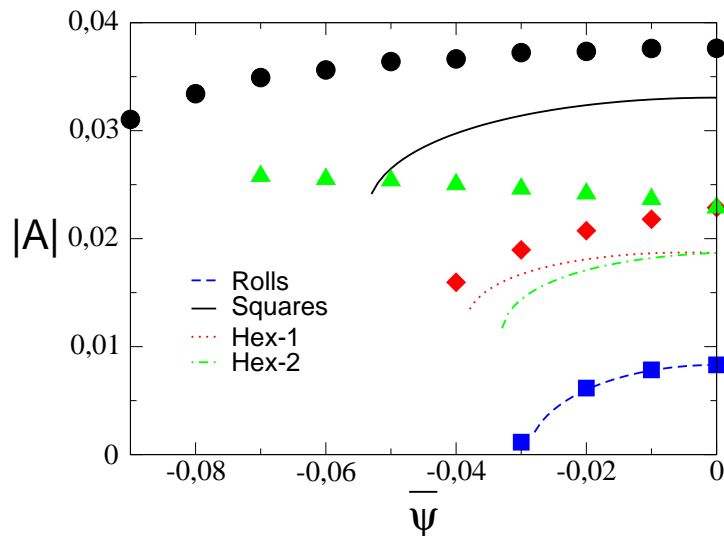


**Figure 4.** Comparison of the magnitude of  $A$  that minimises the free energy as a function of  $\bar{\psi}$  for different patterns. The analytical solutions are plotted as lines. The numerical simulations for rolls, squares, Hex-1 and Hex-2 are plotted as squares, circles, diamonds and triangles, respectively.

in one unit cell with initial conditions listed in equation (13). The free energy is evaluated numerically using equation (12) after the numerical solution reaches a steady state. Since the wave number  $q$  that minimises the free energy depends on  $\bar{\psi}$ , the simulation for each pattern at a fixed value of  $\bar{\psi}$  is repeated with a different system size until the minimum of the free energy is found.

A comparison of the amplitudes of the principal reciprocal lattice vectors obtained from the numerical simulations and the corresponding analytical solution is shown in figure 4. In the numerical simulations, the amplitudes of the principal reciprocal lattice vectors are computed using the Fourier transform. For rolls, the one-mode approximation and the numerical simulations are in good agreement. This is reasonable because the next-nearest reciprocal lattice vectors of rolls are  $\langle 20 \rangle$ , which is far from the  $\langle 10 \rangle$  principal reciprocal lattice vectors. This makes them difficult to excite, and the one-mode approximation is quite accurate. In contrast, for squares and hexagons, the higher-order reciprocal lattice vectors are closer to the principal reciprocal lattice vectors (e.g.,  $\langle 11 \rangle$  for squares), and thus the one-mode approximation and the numerical simulations do not agree as well. Thus, an analytical calculation including higher-order modes is required to give more accurate predictions. Nevertheless, the one-mode approximation gives a good qualitative prediction of the relative values of the free energies at the end point of the solid solution branches, as well as for the intersection points of solid and liquid free energy curves.

The free energy difference  $f - f_L$  is plotted in figure 5. This difference is so small that it would be difficult to distinguish the free energy curves if they were plotted as in figure 2. The one-mode approximation and numerical simulations show the same

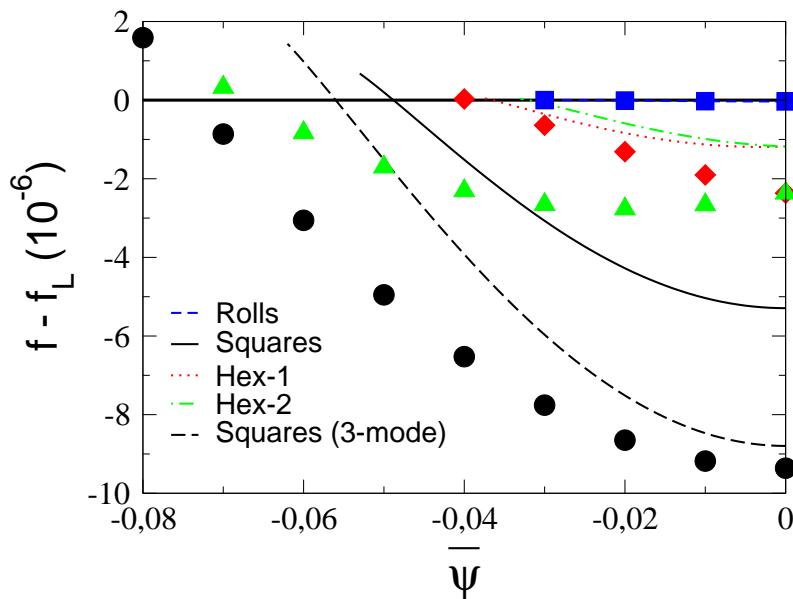


**Figure 5.** Comparison of the free energy densities as a function of  $\bar{\psi}$  for different patterns. Symbols and lines as in figure 4.

ordering of the intersection points of solid and liquid free energy curves, as in figure 4, namely  $|\bar{\psi}_{\text{square}}^{\text{int}}| > |\bar{\psi}_{\text{hex}}^{\text{int}}| > |\bar{\psi}_{\text{roll}}^{\text{int}}|$ . In addition, for the parameters chosen above, rolls and hexagons are metastable states and the square lattice is the ground state for a wide range of  $|\bar{\psi}|$  until it loses its stability to liquid at  $|\bar{\psi}| = 0.073$ . To illustrate the influence of triadic interactions on the free energy calculation, a three-mode approximation that considers  $\langle 10 \rangle$ ,  $\langle 11 \rangle$  and  $\langle 12 \rangle$  reciprocal lattice vectors for the square lattice is computed and shown in figure 5.

To simulate solid-liquid coexistence, we set the simulation parameters to  $\Delta x = \Delta y = 0.53$  on a system of size  $L_x = 384\Delta x$  and  $L_y = 192\Delta y$  with periodic boundary conditions. The initial condition for the density is

$$\psi = \frac{1}{2} \left( 1 + \tanh \left( x - \frac{L_x}{2} \right) \right) \psi_S(\vec{r}) + \frac{1}{2} \left( 1 - \tanh \left( x - \frac{L_x}{2} \right) \right) \bar{\psi}_L, \quad (27)$$

where  $\psi_S$  is the one-mode approximation of square lattices as shown in equation (13), and  $\bar{\psi}_L$  is the constant density of the liquid. The average densities of solid and liquid are chosen to be close to  $\bar{\psi}_{\text{square}}^{\text{int}}$ , which is determined numerically. The initial amplitude of the square lattice is set to the value obtained from the steady state square lattice simulations at the same average density. Uniformly distributed random fluctuations of the magnitude of half the square pattern amplitude are applied initially to examine the stability of the square pattern. The simulations show that the square-liquid coexistence is stable against the initial random fluctuations, and the equilibrium solid-liquid coexistence is shown in figure 6. Furthermore, it can be seen in figure 6 that the square-liquid interface displays different spatial decay rates for the different density waves as predicted by the classical density functional theory of freezing. In particular,

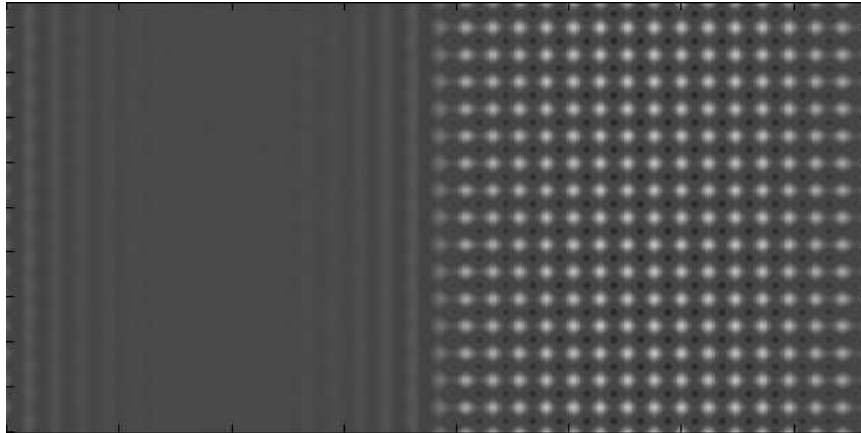


**Figure 6.** Square-liquid coexistence simulated using the free energy functional shown in equation (12).

the density wave of  $\langle 10 \rangle$  decays more slowly into the liquid than the density wave of  $\langle 01 \rangle$  for the  $\{10\}$  interface. The directional dependence of the spatial decay rate of density waves into the liquid was shown to be a main determinant of the anisotropy of interface properties, as discussed in [6, 27].

## 5. Elastic constants

We briefly investigate here the elastic properties of our model. This is important because the analysis of the two-mode model presented in [14] predicts that the shear modulus for square patterns is zero in the limit of small  $\epsilon$  if only the mode corresponding to the principal reciprocal lattice vectors  $\langle 10 \rangle$  is active. Only the addition of the second mode corresponding to the second reciprocal lattice vectors  $\langle 11 \rangle$  ensures a finite and positive shear modulus. Since our model is based on a single unstable mode, it is important to evaluate the shear modulus.

To determine the elastic constants, we follow the lines of earlier work [2, 14] and consider perturbations of the density field given by equation (13). For shear, bulk and deviatoric deformations, we use

$$\psi_{\text{shear}} = \bar{\psi} + 2A (\cos q(x + \xi y) + \cos qy), \quad (28)$$

$$\psi_{\text{bulk}} = \bar{\psi} + 2A \left( \cos \frac{qx}{(1 + \xi)} + \cos \frac{qy}{(1 + \xi)} \right), \quad (29)$$

and

$$\psi_{\text{deviatoric}} = \bar{\psi} + 2A \left( \cos \frac{qx}{(1 + \xi)} + \cos \frac{qy}{(1 - \xi)} \right), \quad (30)$$

respectively, where  $\xi$  is the strain. These expressions are then inserted in the free energy functional (12), which can be explicitly evaluated in terms of  $q$ ,  $A$ , and  $\xi$ . We set the wave number  $q$  equal to the wave number of the reference (unstrained) state,

and determine  $A$  by minimising the free energy of the strained state for each value of  $\xi$  numerically using again the Newton-Raphson method. This value is then used to evaluate the free energy density, as a function of  $\xi$ . The difference with the free energy of the unstrained state,  $\Delta f$ , can be related to the elastic constants. To lowest order in  $\xi$ , we have

$$\begin{aligned}\Delta f_{\text{shear}} &= \frac{C_{44}}{2}\xi^2 \\ \Delta f_{\text{bulk}} &= (C_{11} + C_{12})\xi^2 \\ \Delta f_{\text{deviatoric}} &= (C_{11} - C_{12})\xi^2.\end{aligned}\tag{31}$$

We have evaluated the free energies of the strained states for the same parameters as the numerical simulations shown previously, except that we set  $\bar{\psi} = 0$  for simplicity. The results indeed display the expected quadratic behaviour for  $\xi \ll 1$ , and the elastic constants are, in our dimensionless units,

$$\begin{aligned}C_{11} &= 7.8 \times 10^{-3}, \\ C_{12} &= 1.1 \times 10^{-3}, \\ C_{44} &= 1.63 \times 10^{-4}.\end{aligned}\tag{32}$$

The shear modulus is  $\mu = C_{44} = 1.63 \times 10^{-4}$ , and the (two-dimensional) bulk modulus  $B = (C_{11} + C_{12})/2 = 3.85 \times 10^{-3}$ . The ratio of the bulk modulus and the shear modulus is about 24.

Thus, for the parameters chosen here the square patterns generated by our model are rather “soft” with respect to shear deformation, but have a perfectly well-defined finite shear modulus. Several remarks can help to understand this fact. A shear deformation corresponds, in reciprocal space, to a change of the angle between reciprocal lattice vectors, whereas their length remains unchanged to first order in  $\xi$ . Since we have found that the free energy depends on this angle if anisotropic terms are present according to equation (9), this directly gives a finite contribution to the shear modulus. Note, however, that this is not the only contribution. Indeed, since the change in the angle modifies the strength of the nonlinearities which saturate the density waves, the amplitude  $A$  also depends on the deformation, which modifies the contributions of all the other terms in the functional. Furthermore, the nature of the bifurcation also comes into play. For a subcritical bifurcation,  $A$  can be appreciable even for small  $\epsilon$ , which means that the anisotropic terms, though proportional to  $A^4$  or  $A^6$ , may be comparable to the quadratic contribution which determines the elastic constants in the standard PFC model.

Note that the above calculation of the elastic constants uses the one-mode approximation, which is not very accurate in view of the results shown in figure 4. However, it is sufficient for our main purpose here, which was to demonstrate that the shear modulus is finite. For a more quantitative evaluation of the elastic constants, multi-mode calculations or direct numerical computations are mandatory. Furthermore, we have evaluated the elastic constants here only for one specific set of coefficients. How

they depend on the various parameters in the free energy functional is an interesting subject for further investigations.

## 6. Conclusions

We have presented a general method of constructing a free energy functional for the PFC model that exhibits solid-liquid coexistence with desired crystal symmetries. We have demonstrated that the crystal symmetries in the PFC model can be controlled through additional nonlinear terms. In particular, we have examined the influence of nonlinearities such as  $g_{2n}\psi^2\Delta^n\psi^2$  and  $s_{2m}|\nabla\psi|^{2m}$  on crystal symmetries. Besides the squares that have been investigated here, other structures can potentially be obtained by using terms with  $n \geq 4$ , since these terms contain higher order harmonics that can be used to favour well-defined angles between density waves.

We have also presented a systematic procedure for constructing free energy functionals that exhibit square-liquid coexistence as the ground state. This requires (i) a subcritical bifurcation from the liquid to the square state, and (ii) a suitable combination of the nonlinear coefficients which favours squares over rolls and, at the same time, makes triadic resonances small enough to avoid hexagons. Our analytical results obtained in the one-mode approximation are borne out qualitatively by numerical simulations: in both simulations and analytics the square lattice is the ground state until it loses its stability to the liquid at large  $|\bar{\psi}|$ . The one-mode approximation, however, does not predict accurately the amplitude and free energy for square lattices. A multi-mode approximation is needed to quantitatively describe the square symmetry since the principal lattice vectors of the square lattice are strongly coupled to higher order modes. Nevertheless, the one-mode analysis provides a good guideline for determining coefficients of nonlinearities to obtain the desired crystal symmetries.

We have obtained stable square-liquid coexistence, and the solid exhibits a finite shear modulus, which makes this model suitable for simulations. A drawback is that several nonlinear terms are needed, and that a delicate balance between the coefficients needs to be respected. We have only tested one specific set of coefficients, but we expect that the properties of the model (elastic constants, interfacial properties) can be varied by exploring the parameter space of the various coefficients. It should also be noted that our survey of potential nonlinear terms is by no means complete. However, the relation between the coefficients and the resulting model properties is highly non-trivial, which implies that the process of finding a set of coefficients that yield a match with some desired materials properties is likely to be cumbersome. Furthermore, our final equation of motion (25) is of 8th order in space, which is only two orders lower than the one of the two-mode model [14].

A highly interesting perspective is the extension of this work to three dimensions. The calculation of the anisotropy performed in section 2 remains valid in three dimensions, which means that it is straightforward to obtain simple cubic structures. Furthermore, since it has been found that the free energies of bcc, fcc, and hcp phases



in three dimensions in the standard PFC model are not very different for a certain range of  $\epsilon$  [10, 11, 12], the addition of anisotropic terms may be used to control their relative stability.

## Acknowledgments

This work was supported by joint funding under EU STRP 016447 MagDot and NSF DMR Award No. 0502737.

## Appendix A. Inequalities for the coefficients in the free energy functional

Here, we give the details concerning the calculation of the intersection points between liquid and solid free energies and the resulting conditions for the coefficients in the free energy functional. We start with rolls and squares. As outlined in section 3.2, we need to compare the values of  $\beta^2/(4N\gamma)$ , where  $\beta$ , and  $\gamma$  are the coefficients of equation (17) for a generic subcritical bifurcation. Comparing equations (14) and (15) to equation (17), we obtain the coefficients  $\beta$  and  $\gamma$  for rolls and squares,

$$\begin{aligned}\beta_{\text{roll}} &= \frac{1}{2}(-3 - 3s_4q^4 + \lambda_1\Xi), \\ \gamma_{\text{roll}} &= \frac{10}{3}s_6q^6,\end{aligned}\tag{A.1}$$

$$\begin{aligned}\beta_{\text{square}} &= (-9 - 5s_4q^4 + \Xi), \\ \gamma_{\text{square}} &= \frac{56}{3}s_6q^6,\end{aligned}\tag{A.2}$$

where

$$\begin{aligned}\Xi &\equiv -32g_4q^4 + 96g_6q^6, \\ \lambda_1 &\equiv (-16g_4q^4 + 64g_6q^6)/\Xi.\end{aligned}\tag{A.3}$$

The subcritical bifurcation requires the quartic coefficient to be negative, which according to equation (11) implies

$$\beta_{\text{square}} > 0.\tag{A.4}$$

This determines an upper bound for  $s_4$ ,

$$s_4q^4 < \frac{-9 + \Xi}{5}.\tag{A.5}$$

The condition that the intersection of the square and liquid free energy curves occurs at a higher value of  $|\bar{\psi}|$  than that of rolls and liquid (i.e.,  $|\bar{\psi}_{\text{square}}^{\text{int}}| > |\bar{\psi}_{\text{roll}}^{\text{int}}|$ ), yields

$$\frac{\beta_{\text{square}}^2}{8\gamma_{\text{square}}} > \frac{\beta_{\text{roll}}^2}{4\gamma_{\text{roll}}},\tag{A.6}$$

which can be reduced to the inequality

$$99 - 25\Xi + 42\lambda_1\Xi - \sqrt{\Omega_1} < s_4q^4 < 99 - 25\Xi + 42\lambda_1\Xi + \sqrt{\Omega_1},\tag{A.7}$$

where

$$\Omega_1 = 70(5\lambda_1\Xi - 3\Xi + 12)^2. \quad (\text{A.8})$$

The solution of  $s_4q^4$  exists only if the upper bound of  $s_4q^4$  obtained from equation (A.5) is greater than the lower bound obtained from equation (A.7), which yields

$$(-9 + \Xi)/5 > 99 - 25\Xi + 42\lambda_1\Xi - \sqrt{70} |5\lambda_1\Xi - 3\Xi + 12|. \quad (\text{A.9})$$

The above inequality holds if (a)  $\lambda_1 < 3/5$  and  $\Xi > 12/(3 - 5\lambda_1)$  or (b)  $\lambda_1 > 3/5$  and  $\Xi < 12/(3 - 5\lambda_1)$ . It is helpful to rewrite the expression of  $\lambda_1$  as

$$\lambda_1 = \frac{3}{5} + \frac{4}{5} \cdot \frac{4g_4q^4 + 8g_6q^6}{\Xi}. \quad (\text{A.10})$$

For the case that  $g_6 = 0$ , we have  $\lambda_1 = 3/5 - 1/10 < 3/5$  and the solution of  $s_4$  only exists if  $\Xi > 12/(3 - 5\lambda_1) > 0$ . However, this requires  $g_4$  to be negative which contradicts the condition for stable liquid shown in equation (21). Thus it is essential to include the nonlinear term  $\psi^2\Delta^3\psi^2$  in the free energy functional so that the free energy functional exhibits the desired properties of (i) stable liquid, (ii) subcritical bifurcation, and (iii)  $|\bar{\psi}_{\text{square}}^{\text{int}}| > |\bar{\psi}_{\text{roll}}^{\text{int}}|$ .

For hexagons, the coefficients  $\alpha$ ,  $\beta$ , and  $\gamma$  are given by equation (24). The coefficient  $\tau$  of the cubic term is assumed to be small, such that this term can be neglected. Then, the condition that  $|\bar{\psi}_{\text{square}}^{\text{int}}| > |\bar{\psi}_{\text{hex}}^{\text{int}}|$  requires

$$\frac{\beta_{\text{square}}^2}{8\gamma_{\text{square}}} > \frac{\beta_{\text{hex}}^2}{12\gamma_{\text{hex}}}, \quad (\text{A.11})$$

yielding the inequality

$$-45 + 65\Xi + 24\lambda_2\Xi - \sqrt{\Omega_2} < s_4q^4 < -45 + 65\Xi + 24\lambda_2\Xi + \sqrt{\Omega_2}, \quad (\text{A.12})$$

where

$$\lambda_2 \equiv (84g_4q^4 - 264g_6q^6)/\Xi, \quad (\text{A.13})$$

and

$$\Omega_2 = \frac{52}{9} (10\lambda_2\Xi + 27\Xi - 18)^2. \quad (\text{A.14})$$

Together with equation (A.5), we find that either (a)  $\lambda_2 > -27/10$  and  $\Xi > 18/(27 + 15\lambda_2)$  or (b)  $\lambda_2 < -27/10$  and  $\Xi < 18/(27 + 15\lambda_2)$  has to be fulfilled in order to make  $|\bar{\psi}_{\text{square}}^{\text{int}}| > |\bar{\psi}_{\text{hex}}^{\text{int}}|$ .

## References

- [1] Elder K R, Katakowski M, Haataja M and Grant M 2002 *Phys. Rev. Lett.* **88** 245701
- [2] Elder K R and Grant M 2004 *Phys. Rev. E* **70** 051605
- [3] Swift J and Hohenberg P C 1977 *Phys. Rev. A* **15** 319
- [4] Cross M C and Hohenberg P C 1993 *Rev. Mod. Phys.* **65** 851
- [5] Elder K R, Provatas N, Berry J, Stefanovic P and Grant M 2007 *Phys. Rev. B* **75** 064107
- [6] Wu K-A and Karma A 2007 *Phys. Rev. B* **76** 184107
- [7] van Teeffelen S, Löwen H, Backofen R and Voigt A 2009 *Phys. Rev. E* **79** 051404

- [8] Ramakrishnan T V and Youssouff M 1979 *Phys. Rev. B* **19** 2775
- [9] Singh Y 1991 *Phys. Reports* **207** 351
- [10] Tegze G, Gránásy L Tóth G I, Podmaniczky F, Jaatinen A, Ala-Nissila T and Pusztai T 2009 *Phys. Rev. Lett.* **103** 035702
- [11] Tóth G I, Tegze G, Pusztai T, and Gránásy L 2010 this volume
- [12] Jaatinen A and Ala-Nissila T 2010 this volume
- [13] Lifshitz R and Petrich D M 1997 *Phys. Rev. Lett.* **79** 1261
- [14] Wu K-A, Adland A and Karma A 2010 Phase-field crystal model for fcc ordering *Preprint* arXiv:1001.1349
- [15] Greenwood M, Provatas N and Rottler J 2010 Free energy functionals for efficient phase field crystal modeling of structural phase transformations *Preprint* arXiv:1002.3185
- [16] Busse F H 1978 *Rep. Prog. Phys.* **41** 1930
- [17] Gertsberg V L and Sivashinski G I 1981 *Prog. Theor. Phys.* **66** 1219
- [18] Bestehorn M and Haken H 1984 *Z. Phys. B* **57** 329
- [19] Herrero H, Pérez-Garcia C and Bestehorn M 1994 *Chaos* **4** 15
- [20] Kubstrup C, Herrero H and Pérez-Garcia C 1996 *Phys. Rev. E* **54** 1560
- [21] Matsushita N and Ohta T 1998 *J. Phys. Soc. Japan* **67** 1973
- [22] Enomoto Y, Oba K, Hayase Y and Ohta T 2001 *J. Phys. Soc. Japan* **70** 2939
- [23] Boyer D and Romeu D 2005 *Int. J. Mod. Phys. B* **19** 4047
- [24] Sakaguchi H and Brand H R 1997 *Europhys. Lett.* **38** 341
- [25] Crawford C and Riecke H 1999 *Physica D* **129** 83
- [26] Mellenthin J, Karma A and Plapp M 2008 *Phys. Rev. B* **78** 184110
- [27] Wu K-A, Karma A, Hoyt J J and Asta M 2006 *Phys. Rev. B* **73** 094101